Journal of Sol-Gel Science and Technology (2020) 93:479–494
https://doi.org/10.1007/s10971-019-05054-8

REVIEW PAPER: SOL–GEL AND HYBRID MATERIALS FOR DIELECTRIC, ELECTRONIC, MAGNETIC AND FERROELECTRIC APPLICATIONS

An overview of La_2NiMnO_6 double perovskites: synthesis, structure, properties, and applications

Aslam Hossain[1] · A. K. M. Atique Ullah[2] · Partha Sarathi Guin[3] · Sanjay Roy[3]

Received: 16 January 2019 / Accepted: 14 June 2019 / Published online: 5 July 2019

Abstract

Multifunctional materials having simultaneous electrical and magnetic assembling have been attempted by numerous researchers for next-generation electronic appliances. Among such materials, rare earth metals containing double perovskites, such as $La_2BB'O_6$ (B = Ni, B′ = Mn) are the utmost studied materials. In this review, we have summarized various physicochemical aspects of La_2NiMnO_6 such as crystal structure, electrical, magnetic, and magneto-transport behavior from earlier studies under several experimental conditions. Magnetic field and temperature effects on magnetoelectric and electronic behavior of this material are described. We discuss how the morphology in the form of bulk phase, thin layer, and nanoparticles affect such physicochemical properties of this material. We also highlighted the role of cation order–disorder at 'B' sites and the probability of the resulting numerous electronic behavior in this type of material and expectation on basic understanding of Ni–O–Mn electronic, as well as magnetic properties. The prospective applications of this material over conventional substances in solar cells, electric tunable devices, biomolecular and gas sensing technologies are also ascribed. The motivation of the present review is to sum up all such behaviors of La_2NiMnO_6 to find its possible applications in new areas of material research and the directions of future works.

✉ A. K. M. Atique Ullah
atique.chem@gmail.com

✉ Partha Sarathi Guin
parthasg@gmail.com

✉ Sanjay Roy
sanjayroyp@gmail.com

[1] Department of Physical and Inorganic Chemistry, Institute of Natural Science and Mathematics, Ural Federal University, Yekaterinburg 620000, Russia

[2] Nanoscience and Technology Research Laboratory, Atomic Energy Centre, Bangladesh Atomic Energy Commission, Dhaka 1000, Bangladesh

[3] Department of Chemistry, Shibpur Dinobundhoo Institution (College), Howrah 711102, India

Graphical Abstract

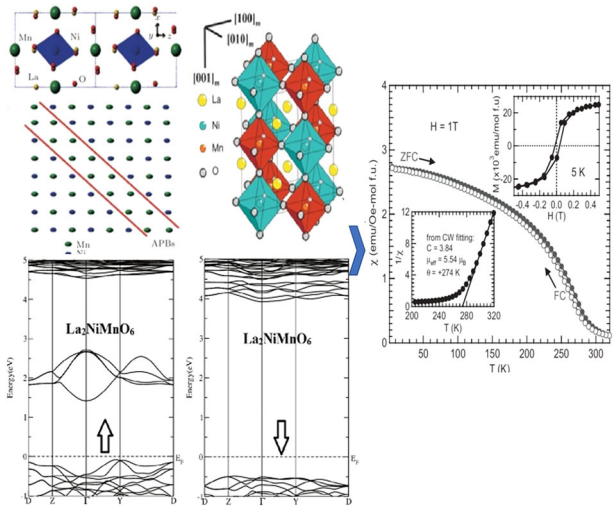

Highlights

- La_2NiMnO_6 double perovskite exhibits simultaneous electric and magnetic orderings
- Crystal structure, magneto-electric, and transport nature affect the functionality of La_2NiMnO_6
- Bulk phase, thin layer, and nanoparticles morphology affect the physical property of La_2NiMnO_6
- La_2NiMnO_6 holds solar cell, electric tunable device, biomolecular and gas sensing applications

Keywords Multifunctional materials · Double perovskites · Crystal structure · Magnetic properties · Electronic properties

1 Introduction

In the current past, attempts have been introduced in producing multifunctional materials with simultaneous electric and magnetic ordering, which is driven mostly by the growing need for the lowering of consumption of power and additional functionality for next-generation electronic appliances [1]. In this case a strong magnetoelectric coupling is essential for useful applications though the observed strength for intrinsic coupling in such multifunctional materials is generally literally small. It is well established that magnetoelectric coupling exists in a multiferroic composite which consists piezoelectric and piezomagnetic phases with 0–0 and 1–1 connectivity. It is imperative to talk about that such substances are rare as the electronic origins of spontaneous magnetic and electric dipolar ordering are commonly exclusive [2]. Considerable magneto dielectric effect has been detected in spin-spiral systems in recent times such as $TbMnO_3$ [1] and CuO [3] at desire temperatures and even below room temperature, and same effect has also been detected in charge-ordered arrangement like $LuFe_2O_4$ [4]. Yang et al. [5]. have mentioned that the magnetodielectric effect in that system is dynamically improved because of the control of magnetic field of the dielectric relaxation.

Owing to interesting properties and broad potential functioning multiferroic materials having coexistence of minimum two ferroic behaviors have been deliberated widely [6]. R_2NiMnO_6 (where, R = Pr, Nd, Sm, Gd, and Ho) are a particular set of oxides of double perovskite [7] in which a near-ideal e_g^2–O–e_g^0 electronic exchange leads to ferromagnetic coupling of d-electron spins in accordance to the very well-known established Goodenough–Kanamori rules [8, 9]. It is to be noted that the general formula of double perovskites is $A_2(BB')O_6$, where A stands for an alkali-earth metal and B, B' are transition metals. These materials have many potential applications because of their substantial behaviors such as sensors, memory devices, radio frequency filters, and phase shifters. The magnetroresistance, colossal magneto-dielectricity and room temperature ferromagnetic insulating properties allow La_2NiMnO_6 as a potential candidate for alternative magnetoelectric material. In addition, the inherent intrinsic lattice strain of the biphasic composition compounds has attracted considerable interest to the researchers in this research area [10]. The probability of the resulting numerous electronic behavior in this material and expectation on basic understanding of Ni^{2+}–O–Mn^{4+} electronic interaction would provide new tracks for designing the multiple property materials.

Among the perovskites, multifunctional double perovskite oxides containing rare-earth elements such as $La_2BB'O_6$ (B = Ni; B′ = Mn) are the most usually studied materials due to their enriched technological aspects [10]. An ordered double perovskite such as La_2NiMnO_6 is a ferromagnetic semiconductor having $T_C = 280$ K. Studies on bulk La_2NiMnO_6 have expressed enormous magnetic field induced variations in the dielectric behaviors and resistivity at temperatures at and above 280 K [10]. This temperature is quite higher than earlier observation for such a coupling of magnetic, dielectric, and electric properties in a ferromagnetic semiconductor. Such properties arising out of possible combination of multiple electronic behavior like ferromagnetism, magnetoresistance, magneto capacitance, and semi-conductivity involving Ni^{2+}–O–Mn^{4+} electronic interaction in this substance provide a new guideline in designing new multiple property materials.

In this review, crystal structure, electrical, magnetic, and magneto-transport properties of La_2NiMnO_6 are accumulated from earlier studies. The goal of the current article is to recapitulate the physicochemical behavior of La_2NiMnO_6, which have been investigated till now. Based on these properties, the possible applications and the direction of future research in this field are furnished.

2 Bulk materials

2.1 Synthesis and crystal structural feature

The double perovskite compound, $A_2(BB')O_6$, where A refers to an alkali-earth metal and B, B′ are transition metals. It is well known that the cation order–disorder plays a potential role in governing the crystal geometry and behavior of several complex perovskites type oxides. It has been perceived that various physicochemical behavior like superconductivity, ferroelectricity, colossal magnetoresistance, magnetic ordering, multiferroic property, piezoelectricity, ionic or electronic conductivity are dependent strongly on the extent of order of A and/or B sites. Generally, B/B′ ordered distribution is stabilized when B and B′ cations vary considerably regarding their charge and size [11]. By choosing Ni^{2+} and Mn^{4+} and with the help of charge differences the complete B-site ordering may be attained in designed double perovskite La_2NiMnO_6. In many earlier studies it has been detected that in a well-ordered La_2NiMnO_6, a rhombohedral or a monoclinic symmetry with Ni^{2+} and Mn^{4+} which are alternatively arranged at B sites, whereas in a disordered phase there is an orthorhombic symmetry with a random distribution of Ni^{3+} and Mn^{3+} at the sites, B of ABO_3 perovskite. Several authors currently worked on La_2NiMnO_6 and explained the variations of properties on synthetic condition. The summaries of relevant experimental conditions and crystallographic data were shown in Table 1.

La_2NiMnO_6 is biphasic in nature, which exists at high temperature in rhombohedral phase, whereas it transforms at room temperature to monoclinic or orthorhombic. At low temperature, material's rhombohedral phase changes to later subjected to the Ni/Mn B-site sub-lattice arrangement [11]. The random arrangement of Mn and Ni over the octahedral sites of perovskite structure is found to happen for rhombohedral *R-3c* and orthorhombic *Pbnm*, whereas an ordering of Mn and Ni into a distinguishable site may be arranged in rhombohedral *R-3* or *R-3m* and monoclinic *P21/n* space groups. Both the rhombohedral and orthorhombic or monoclinic phases of La_2NiMnO_6 have been observed to co-exist over a wide-ranging of temperature, including room temperature [9]. La_2NiMnO_6 has a typical double perovskite structure with two different B-sites, as shown in Fig. 1a [12]. In the bulk La_2NiMnO_6 sample, Mn and Ni are normally ordered in the matter of occupying B-site, as shown in Fig. 1b [12]. The basic structure of La_2NiMnO_6 showing ordered monoclinic geometry is shown in Fig. 1a [13] and the crystallographic structure is shown by Fig. 1c. However, the boundary atoms of different domains are the same, being either Mn or Ni in the structural domains of the materials. In case two such domains gather, an interface known as anti-site phase boundary is generated [14, 15], containing either Ni–O–Ni or Mn–O–Mn bonds only, as shown in Fig. 1a, b. In the fully ordered La_2NiMnO_6, ions of Mn and Ni exist as Mn^{4+} and Ni^{2+}, however, in the fully disordered $LaNi_{0.5}Mn_{0.5}O_3$ (113 phase), they exist as Mn^{3+} and Ni^{3+} showing different crystal structures. Previous study has depicted that Ni^{2+} and Mn^{4+} are major in the compound while a little proportion of Ni^{3+} and Mn^{3+} coexist in La_2NiMnO_6 depending upon the conditions of sample synthesis [11].

The initial report on La_2NiMnO_6 has revealed that the material crystallizes in orthorhombic crystal symmetry with slight monoclinic distortion prepared at 1100 °C [16]. The compound synthesized at temperature higher than 1300 °C is crystallized as monoclinic structure [11, 17]. The structure of La_2NiMnO_6 is rhombohedral (*R3*) at far higher temperature which at low temperature changes to monoclinic (*P21/n*) and over a wide-ranging of temperature, there is a co-existing of the two structures [18]. Farheen et al. [19] have verified how the variations of annealing temperature and atmosphere affect the properties and crystal structures of La_2NiMnO_6. Figure 2 displays the XRD patterns of the multiphase compounds annealed in different atmospheres such as nitrogen, oxygen, and air [19]. It is also established that the annealing condition affects the orthorhombic distortion of the cation disordered lattice due to the oxygen non-stoichiometry effect.

Table 1 Reported crystallographic data with synthetic conditions

Synthesis	Condition	Space group		a	b	c	β	Ref.
Pechini method	1350 K, 6 h, Air	*P21/n*		5.517	7.748	5.466	90.01	[11]
Modified nitrate decomposition	1373 K, 16 h, Air	*P21/n*		5.467	5.510	7.751	90.12	[18]
Pechini method	1623K, 12 h, Air	*Pbnm*		5.501	5.470	7.751	90	[129]
Standard solid-state reaction	1673K	58% *P21/n* 43% *R-3*						[130]
Sol-gel method	1173 K, 2d, Oxygen	66% *R3c*	34%	5.504	–	12.326		[22]
		Pbnm		5.501	5.450	7.736		
Sol-gel method	1673 K, 12 h, Air	42% *R3c*	58%	5.504	–	13.235		[22]
		Pbnm		5.503	5.452	7.727		
Sol-gel method	1273 K, 12 h	32% *R3c*	68%	5.512	–	13.236		[22]
	Arg	*Pbnm*		5.512	5.458	7.739		
Standard solid-state reaction	1573 K, 4d, Air	*Orthorhombic*		5.477	5.464	7.670	90	[35]
Glycine-nitrate	473 K, 12 h, Air	*Orthorhombic*		5.50	5.650	7.78	90	[35]
Co-precipitation	1023–1373 K,	*Monoclinic*		5.467	5.510	7.751	91.12	[100]
Sol-gel	873–1273 K, 2 h, Air	*Pbnm*		5.515	5.430	7.750	90	[67]
Gel combustion	Air	*R-3* 69%	*P21/n*	5.496	5.475	13.214	89.66	[19]
		31%		5.438		7.747		
Gel combustion	O_2	*R-3* 50%	*P21/n*	5.508	5.473	13.220	89.48	[19]
		50%		5.468		7.751		
Gel combustion	N_2	*Monoclinic*		5.482	5.501	7.770	89.45	[19]
		Orthorhombic (La_2NiO_4)		5.468	5.506	12.675	90	
		Cubic(NiO)		4.1778	4.1778	4.177	90	
	1273–1423 K	*P21/n*		5.509	5.456	7.770	89.82	[33]

La_2NiMnO_6 with the usual structure of double ordered perovskites ($A_2BB'O_6$) is distorted from the standard double perovskite where the change of temperature affects the magnitude of change of distortion. The preparation technique and post heat treatment of the compound affect the cations ordering or disordering in La_2NiMnO_6 lattices. The cation ordering in these perovskites is determined by the octahedral cations' charges and ionic radii differences. However, cation disordering is occurred due to the ionic radii similarity of Mn and Ni, whereas their valence states result in cation ordering in La_2NiMnO_6 lattice. The concurrent lattice ordering and disordering allow La_2NiMnO_6 to show different symmetries which in turns to be magnetically complicated. Consequently, it is challenging to obtain double perovskites multiferroic materials. Thus, the magnetic behavior and cationic ordering of bulk La_2NiMnO_6 is a subject of study in plenty of researches. Various reports have displayed the absence of any cation ordering in La_2NiMnO_6 lattice, whereas other investigations have expressed lattices with partially or fully cation ordered. Previously reported crystallographic data with the conditions of synthesis are shown in Table 1.

2.2 Theoretical predictions of electronic properties

Energy band structure is important to explore the electronic behavior of a compound. Ullah et al. have calculated [20] the band structure along high symmetry points in reduced zone scheme using GGA + U [21] approximation for La_2NiMnO_6 (Fig. 3) to show the indirect band behavior of spin down and spin up states each. The minima of conduction band have been found to arise at the Γ symmetry point whereas the maxima of valence band have been found near the Y symmetry point inside the Brillion zone for spin up state. This gives rise to an indirect band gap (Γ-Y) for spin up state with the band gap value of 1.6 eV. Likewise, the minima of the conduction band are observed to be found at Γ symmetry point while the maxima of the valence band recline along Z symmetry point of Brillouin zone for spin down state. The band gap formed along Γ-Z symmetry

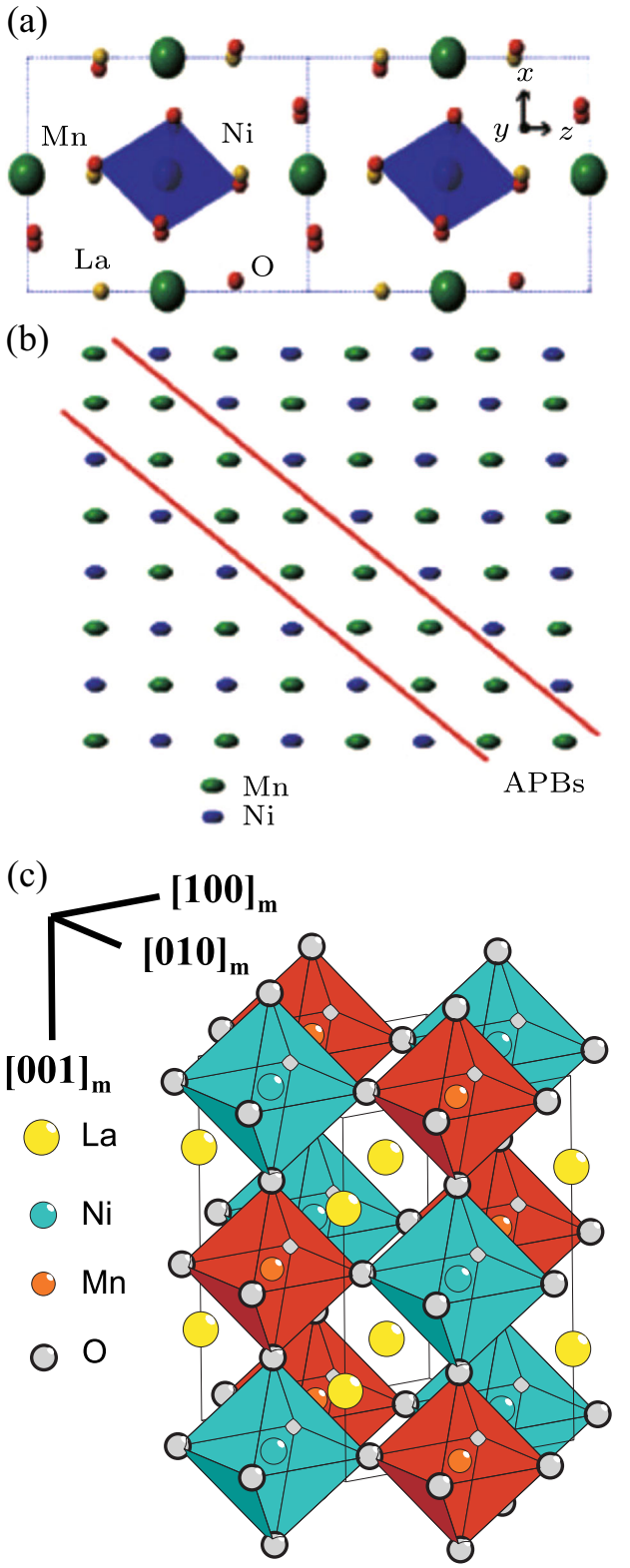

Fig. 1 **a** Schematic illustration of the crystal structure, **b** the differently ordered antisite phase boundary and domain, and **c** crystallographic structure of La_2NiMnO_6 [Reprinted with permisssion from Ref. 12, Copyright Chin. Phys B, 2013, 13]

points is responsible for indirect band nature of the compound in case of spin down state. The band gap energy for La2NiMnO6 has been estimated as 4.4 eV.

According to the calculation of the density of states (DOS), the estimated total and partial DOS for La_2NiMnO_6, the contribution in the valence band from −18 eV to Fermi level is partitioned into three regions for spin down and spins up channels each [20]. The predominant contribution in the energy range of −18 eV to −16.5 eV is for the O-2s state, whereas the contribution of the La-5p state is dominant ranging from −13 eV to −12.2 eV. The major contribution in the region just below Fermi level from −5 eV to 0 eV is for the O-2p state. Above Fermi level, the D-states of La, Ni, and Mn contribute predominantly.

2.3 Experimental and theoretical predictions of magnetic properties

Among various rare earth-based double perovskite compounds, La_2NiMnO_6 is the most widely studied substance for its immense magneto dielectric behavior and transition of ferromagnetic nature at almost ambient temperature (280 K) [10, 11, 22–25]. The previous studies have clearly demonstrated that La_2NiMnO_6 is a ferromagnetic semiconductor, whereas the end components $LaMnO_3$ and $LaNiO_3$ are antiferromagnetic and paramagnetic in nature, respectively [26, 27]. Goodenough et al. [23] have depicted that the ferromagnetism in La_2NiMnO_6 is owing to Mn^{3+}–O–Ni^{3+} super exchange interactions, whereas Blasse [24] has stated that the ferromagnetism is completely due to Mn^{4+}–O–Ni^{2+} super exchange interactions. Other studies on La_2NiMnO_6 have pointed out that the material prepared by solid-state reaction in air has two ferromagnetic (rhombohedral and monoclinic) phases with comparable T_c [11, 18, 28]. Nevertheless, in absence of long-range ordering of Ni and Mn, the most important interactions in La_2NiMnO_6 resulting from Mn–O–Mn and Ni–O–Ni links are antiferromagnetic. In this case, the assumption is the ferromagnetic interaction in disordered octahedral cations occurs by vibrionic super-exchange coupling [5]. Rogado et al. [10] have determined the magnetization with the variation of temperature keeping the field constant and with the variation of applied magnetic field keeping temperature constant. Figure 4a–d demonstrates the magnetic DC and AC susceptibility of La_2NiMnO_6 in different applied field and magnetic transition at 280 K indicating the long-range ordering of ferromagnetic nature [10, 17]. The inset of Fig. 4a demonstrates the inverse susceptibility ($1/\chi$) plot from 300 to 320 K and large θ value obtained (+274 K). This large θ value indicates the strong ferromagnetic interaction between Ni^{2+} and Mn^{2+} spin. Figure 4b shows the low field ZFC and FC magnetization curves where partially disordered La_2NiMnO_6 has sample a ferromagnetic transition

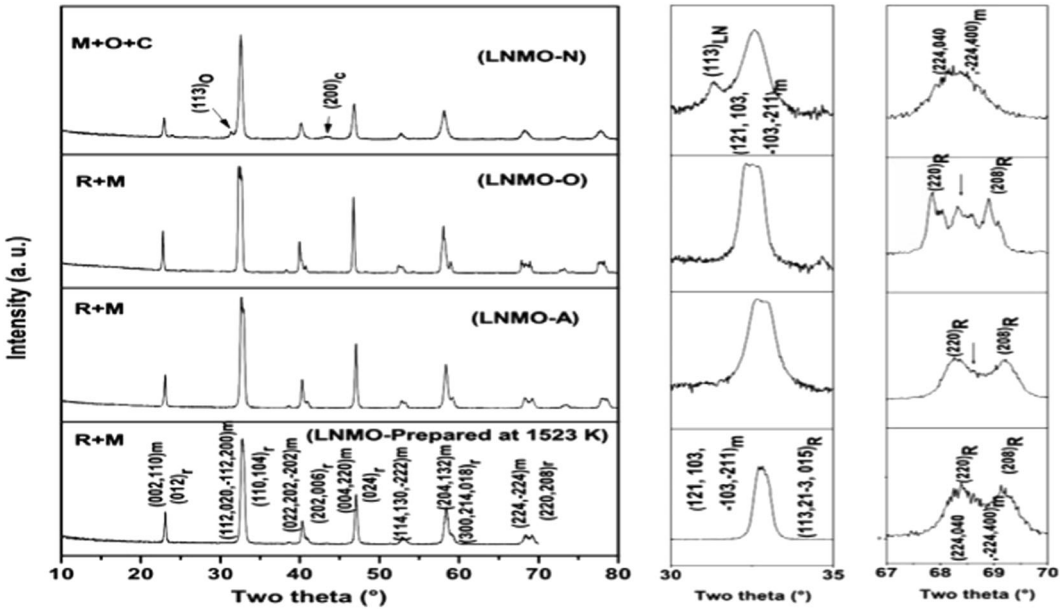

Fig. 2 PXRD patterns of La_2NiMnO_6 annealed in different atmospheres of nitrogen (N), oxygen (O), and air (A). (Subscripts m and r are used to mean monoclinic (M) and rhombohedral (R) phase) [Reprinted with permission from Ref. 19, Copyright 2011, Cambride University Press]

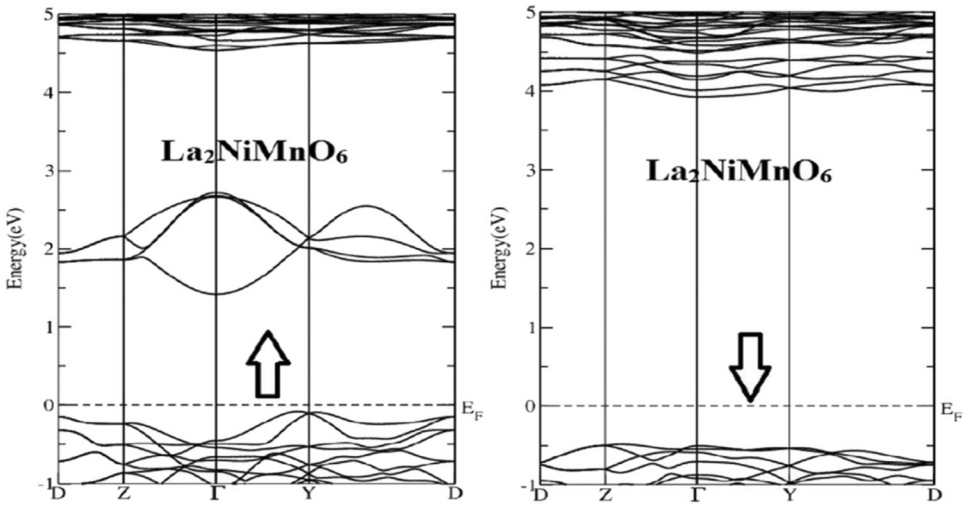

Fig. 3 Band structure estimation of La_2NiMnO_6 for both (left panel) spin up and (right panel) spin down states [Reprinted with permission from Ref. 20, Copyright 2015, Elsevier]

at about 270 K. sharp frequency independent ferromagnetic transition around 270 K and the details of below 150 K are shown in Fig. 4c, d suggest the presence of dynamical features at low temperatures. Figure 4e shows the dip in the difference ZFC plot at T_W for DC memory experiments suggests that La_2NiMnO_6 exhibits spin-glass-like dynamics at low temperatures. So, La_2NiMnO_6 behaves like a re-entrant spin glass or reentrant ferromagnet, exhibiting successive transitions from paramagnetic to ferromagnetic, and ferromagnetic to spin-glass states [17].

By using the first principle DFT-FPAPW method, a ferromagnetic insulating ground state was obtained for La_2NiMnO_6 [29]. The band gap of La_2NiMnO_6 was found as 1 eV, which justifies the semiconducting nature of La_2NiMnO_6. The spin polarized calculations have checked the experimentally observed 5 μB magnetic moment per formula unit. This value fulfills the Hund's first rule for the moments Mn^{4+} ($3d^3$): $t_{2g}^3 e_g^0$and Ni^{2+}(d^8): $t_{2g}^6 e_g^2$. This result also validates the prediction of Goodenough Kanamori (GK) rule that the coupling in between the adjacent $Mn^{4+}$and Ni^{2+}ions are ferromagnetic in nature. The ground states of La_2NiMnO_6 is ferromagnetic semiconducting with alternative Ni/Mn ordering along the (111) direction. Furthermore, it is found that La_2NiMnO_6 is half-metal with Ni/Mn ordering along (001) and (110) after considering the effect of electronic correlation [30]. The determined magnetic moment was 4.7 μB per formula unit which is very much close to the bulk magnetic moment.

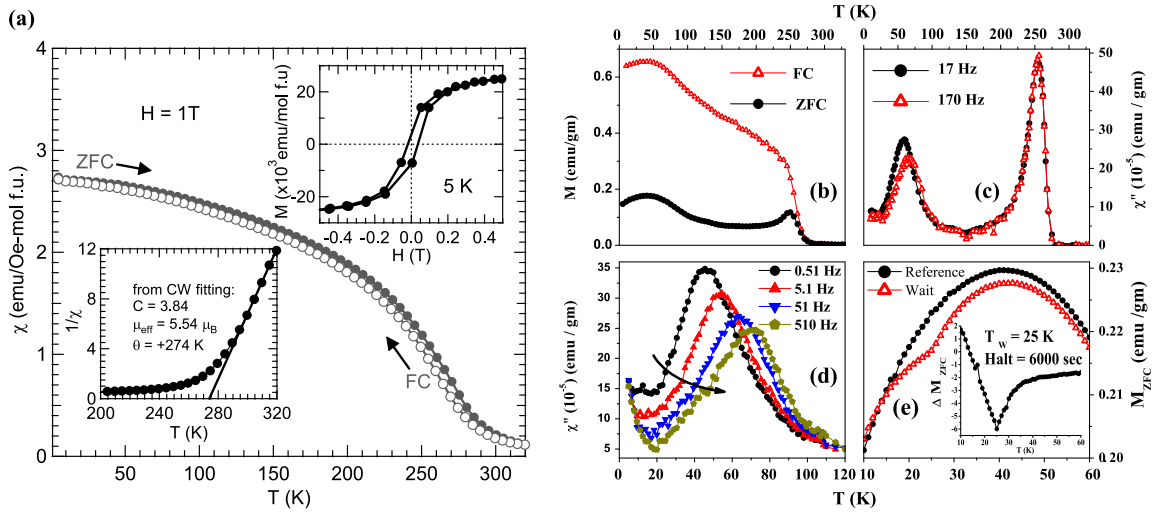

Fig. 4 **a** Magnetic susceptibility χ(T) at 1 T on ZFC and FC. Insets show a plot of 1/χ versus T fitting to the Curie-Weises law (left) and field dependent isothermal magnetization at 5 K (right) [Reprinted with permission from Ref. 10, Copyright 2005, John Wiley and Sons]. **b** FC and ZFC, DC magnetization data at 20 Oe. **c** The imaginary parts of AC susceptibility at H = 4 Oe. **d** The imaginary parts of AC susceptibility at low-temperature. **e** ZFC data with and without an intermediate wait (T_W) at 25 K for 6000 s, (inset showed memory effect) [Reprinted with permkission from Ref. 17, Copyright 2012, Americal Physical Society]

Depending upon the magnetic properties, La_2NiMnO_6 may be classified into three categories such as:

(a) A long range ordered Ni/Mn phase, showing a single transition to paramagnetic from ferromagnetic at about 280 K because of ferromagnetic super-exchange interaction of Mn^{4+}–O–Ni^{2+}. (b) A cation disordered phase with random ordering of the Mn/Ni cations, showing a single transition to paramagnetic from ferromagnetic at about 150 K due to the super-exchange interaction of Mn^{3+}–O–Ni^{3+}. (c) An admixture phase, showing two transitions to paramagnetic from ferromagnetic owing to above mentioned exchange interactions [31].

Thus, it is interesting to see whether the fraction of long range order 2+ and 4+cations on B and B´ sites could be systematically changed by substitution of other cations such as Fe. Since Fe shows 2+ and 3+ valance states, so the existence of Fe affects the percentage of long range ordered cations. In addition, the substitution of Ba^{2+} ions at A site can also force Mn to exist in 4+ state. The results of these types of substitutions introduce reduction in ionic radius and change of valence states and magnetic properties with non-distorted crystal structure. The vacant A site i.e., absence of La by substituting Ba^{2+} also eliminates the probable formation of amorphous La_2O_3 [11, 32].

By introducing first-principles electronic structure calculation, Zhu et al. [30] examined magnetic and electronic natures of La_2NiMnO_6 with Ni/Mn ordering in (*111*), (*110*), and (*001*) directions. They observed that below −2 eV, there are mainly *O-2p* states hybridized with d states of cations, and above 3 eV, there was a narrow peak of La-f states. However, from −2 eV to 3 eV, there are mainly narrow 3d states, in which d states of Ni are lower than those of Mn. The states of d are separated into distinguished e_g and t_{2g} states in a strong octahedral crystal field. Further, they slightly split into five singlet states due to additional weak distortions in *P21/n* monoclinic structure.

Booth et al. [33] have investigated the cation ordered monoclinic R_2NiMnO_6 (where, R = Pr, Nd, Sm, Gd, and Ho) and reported that the FM-Tc is decreased with the decrease in ionic radii of R^{3+} ions. La_2NiMnO_6 exhibits a different polymorphism than the end members ($LaMnO_3$: orthorhombic crystal structure with *Pbnm* (62) space group; and $LaNiO_3$: trigonal crystal structure with *R-3c* space group (167) crystal structures which is due to the differences in crystal structures of the end members. Thus, the cation ordering and the magnetic properties of bulk La_2NiMnO_6 have been a favorable area of research in a many study. Several reports have indicated the absence of cation ordering in the La_2NiMnO_6 lattice while additional studies have reported partially or fully cation ordered lattices [10, 18, 25, 28, 34]. The presence of Mn^{4+}, Mn^{3+}, Ni^{2+}, and Ni^{3+} in the ferromagnetic La_2NiMnO_6 has also been introduced [18, 25, 28]. The neutron diffraction studies revealed the presence of Jahn–Teller distortions in transition metal polyhedra in La_2NiMnO_6 [11, 18].

Sometimes another magnetic transition is found at low temperature range especially for biphasic sample. The low temperature ferromagnetic transition at Tc = 150 K is due the ordering of *Pbnm* phase because of super-exchange interaction involving Mn^{3+}–O–Ni^{3+} [35]. Low temperature spin glass behavior is also reported [17, 36]. The spin glass transition temperature lies around 40 K as found in the temperature-dependent magnetization data [17]. Short range ordering of small ferromagnetic clusters before the actual

arrival of T_C has been explained by Iliev et al. [37], and S. Zhou et al. [38]. Similar short-range ordering and Griffiths phase like property are found in another prototype of the family, Tb_2NiMnO_6 [39]. So, Griffiths like phase may be anticipated in La_2NiMnO_6.

2.4 Magnetoresistance properties

Magnetic field dependent change in resistance of the materials, known as magnetoresistance (MR) effect, has withdrawn a significant attention owing to its enriched physics and technological applications [40–44]. The double perovskite oxide, La_2NiMnO_6, nearly room-temperature ferromagnetic semiconductor, has stimulated much interest owing to its novel electric and magnetic properties [10]. There has been formulated that its ferromagnetic property arises from the superexchange interactions between the alternately ordered Ni^{2+} and Mn^{4+}. However, the inevitable Ni/Mn antisite (AS) disorders will result to the antiferromagnetic (AFM) Ni^{2+}-O^{2-}-Ni^{2+} and Mn^{4+}–O^{2-}–Mn^{4+} configurations [45]. This ferromagnetic material shows antiferromagnetic type interactions. The evaluation of different study predicted that anti-site disorders of bulk La_2NiMnO_6 might be combine with antiphase boundaries. This phenomenon leads to an antiferromagnetic-coupling among the adjacent ferromagnetic domains [46, 47].

This type of behavior has been obtained in various magnetic oxides, e.g., in the granular perovskite, tunneling magnetoresistance (TMR) and in the manganites, the colossal magnetoresistance (CMR) are observed [40, 41]. The spin-dependent tunneling among the ferromagnetic grains originates the TMR effect, which shows an improved low-field response in comparison with the intrinsic TMR effect. Among the tunneling-type MR materials, the introduction of room-temperature low-field MR in double perovskite oxide Sr_2FeMoO_6 has opened a new hope for prospective spintronic devices [42–44]. The research with B-site ordered Sr_2FeMoO_6 have found the magnetic domains of Fe–O–Mo ferromagnetic ordering segregated due to the formation of Fe–O–Fe antiferromagnetic interaction while Fe/Mo anti-site disorder arises. The low field magnetoresistive behavior of Sr_2FeMoO_6 could be attributed to spin dependent tunneling of barriers initiated from the existence of AFM areas [48] While, anti-site disorders are natural growth defect and usually noticed in the family members of double perovskite [34, 49] and attracted attention in other ferromagnetic double perovskites for TMR effect.

Considering the similarity in magnetic structure with those of Sr_2FeMoO_6 and nearly room-temperature FM transition, La_2NiMnO_6 could be a potent candidate of the materials with a nearly room-temperature TMR effect. It has been evidenced that La_2NiMnO_6 exhibits a clear MR effect nearly room-temperature (Fig. 5) and magnetic field dependent MR may be categorized into two sectors as low-field and high-field MR [50]. The experimental results of combine properties of electric and magnetic measurements demonstrated that magnetoresistance at low field can be attributed to tunneling effect between the neighboring ferromagnetic domains where magnetoresistance at high filed could be accredited to restraint of scattering from spin defects due to Ni/Mn AS-disorders.

2.5 Colossal magnetodielectricity

Magnetodielectric materials (Fig. 6) exhibiting dielectric properties at room temperature depending upon the applied

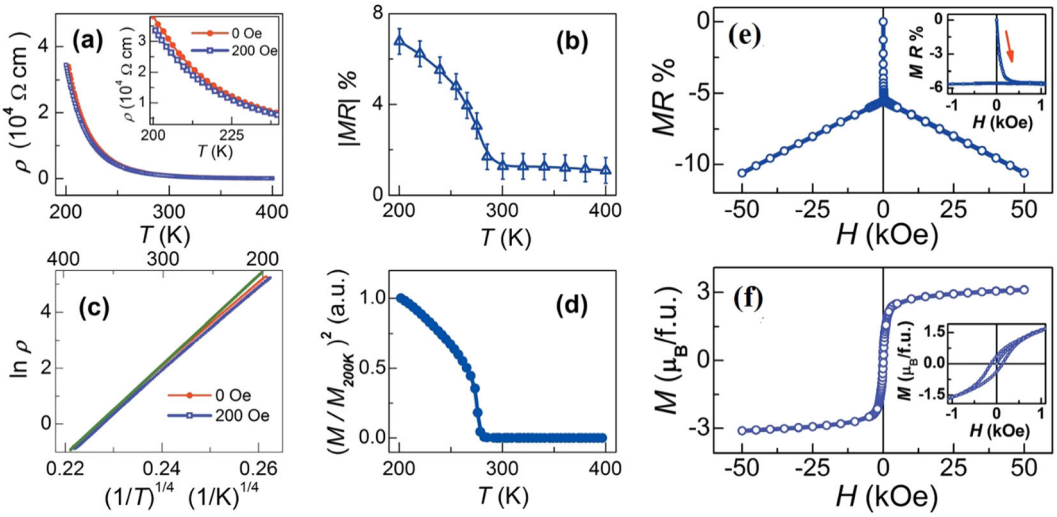

Fig. 5 **a** Temperature dependent resistivity ρ under zero and 200 Oe field at 200 K ≤ T ≤ 400 K. **b** Plot of absolute value of magnetoresisrance versus T. **c** Plots of ln ρ against $(1/T)^{1/4}$. **d** Plot of temperature dependent square of the normalized magnetization $(M/M_{200K})^2$. **e** MR against external magnetic field H at 250 K. **f** Magnetization M versus magnetic field H at 250 K [50]

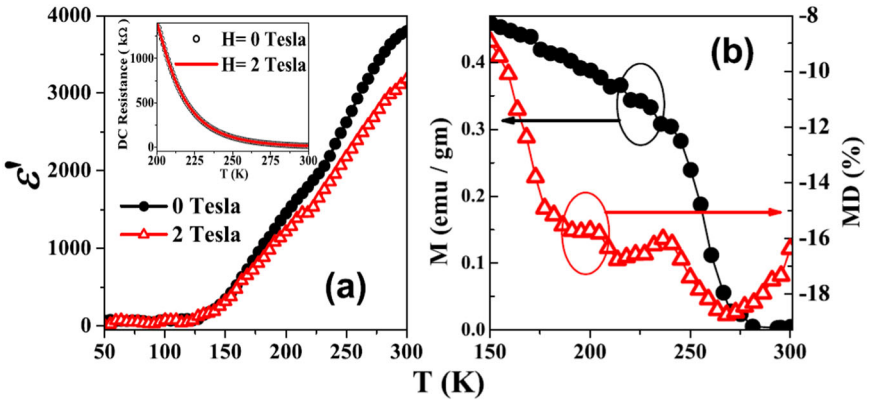

Fig. 6 **a** Dielectric constants at 10 kHz under zero and external field, respectively. **b** Temperature dependent magnetization (left axis, measured with H = 20 Oe) and magnetodielectricity (right axis) [Reprinted with permissions from Ref. 17, Copyright 2012, American Physical Society]

magnetic field are very much encouraging for future device applications [17, 51–53]. Choudhury et al. have shown [17] which partly disordered La_2NiMnO_6 has an array of remarkable behavior like a disordered ferromagnetism at higher temperatures and a reentrant spin-glass transition at lower temperatures, a relaxer-type dielectric behavior, which is a rare example of an intrinsic multi glass system in contrast to Mn-doped $SrTiO_3$ [54, 55]. This is an advanced insulator having colossal magnetodielectric coupling (up to 20%) acting on a wide range of temperature and it is no considerable magnetoresistance property. From this study it has been obtained that the mechanism of asymmetric hopping contributes positively to the dielectric constant. Thus, magnetodielectric coupling may be employed in these types of materials for probing the asymmetric hopping on the relative-spin orientations of adjacent sites. This introduces an innovative path to materialize magnetodielectric materials, which are independent of any type of magnetostriction or electrostriction results.

3 La_2NiMnO_6 thin film

In the recent past, little reports have been prepared to elaborate structural and functional behaviors of thin films of La_2NiMnO_6 unlike the bulk phase of the same material [37, 45, 56–60]. Singh et al. [56, 57] have concluded that at room temperature the films showing multiple magnetic transitions have disordered and ordered phases together and the second magnetic phase transition below 200 K was linked with the disordered parts of films [56, 57]. In other study, Subramanian et al. have established that the optimization of the growth parameters may result a single magnetic transition [61] which has also been reported by Kitamura et al. [60]. Further, these films exhibit a strong spin-lattice coupling and magnetodielectric effect far below the magnetic Curie temperature [10, 37, 62, 63].

The magnetic behaviors of bulk La_2NiMnO_6 have been investigated extensively for last few years to achieve an elaborate knowledge on the behavior of magnetic exchange interactions. Strong magnetodielectric effect in bulk La_2NiMnO_6 [10] and thin films of La_2CoMnO_6 [62] near relevant magnetic transition nearly room temperature expresses the far-reaching technological potential of these materials. However, such strong effect found very near to the FM-T_C of these materials disputes with the magnetodielectric effect of La_2NiMnO_6 thin films [63] found far below the FM-Tc. The absence of long-range structural order probably is a reason for such type of behavior because ordered films show a saturation magnetization close to 4.8 μB/f.u. and FM-Tc around 270 K, while the disordered ones have saturation magnetization, 3.7 μB/f.u. and FM-Tc around 138 K [64]. In such bulk La_2NiMnO_6 and thin films of La_2CoMnO_6, Ni (Co) and Mn ions exchange along precise crystallographic directions over very long distances [65]. It has been stated that this kind of structural order is restricted only to small domain sizes of about 50–100 nm in the thin films of La_2NiMnO_6 [56, 57]. Such studies have established that B-site ordering can play a key role in finding the physicochemical behaviors of double perovskites, especially the coincidence of strong magnetoelectric response and magnetic transition.

The studies on thin films have evidently depicted that there is either a short-range-ordered phase or coexistence of multiple phases like the polycrystalline bulk samples in thin films of La_2NiMnO_6 [37, 45, 56, 57, 59–61]. In fact, the long-range-ordered La_2NiMnO_6 and fully disordered $LaNi_{0.5}Mn_{0.5}O_3$ phases have yet to be stabilized independently in thin-film forms. Such condition also obstructs us to find and analyze their respective functional behavior. Singh et al. [64] have compared the physicochemical behavior of long-range-ordered and completely disordered La_2NiMnO_6 thin films, which were prepared by pulsed-laser deposition. They have detected that ordered and the disordered La_2NiMnO_6 films have different magnetic and electronic behavior, e.g., the magnetic-transition temperatures, low-temperature saturation magnetizations, and phonon-dispersion relations are different for different types of the materials. Wu et al recently epitaxially grown the multiferroic thin films of La_2NiMnO_6 on $SrTiO_3$ (STO),

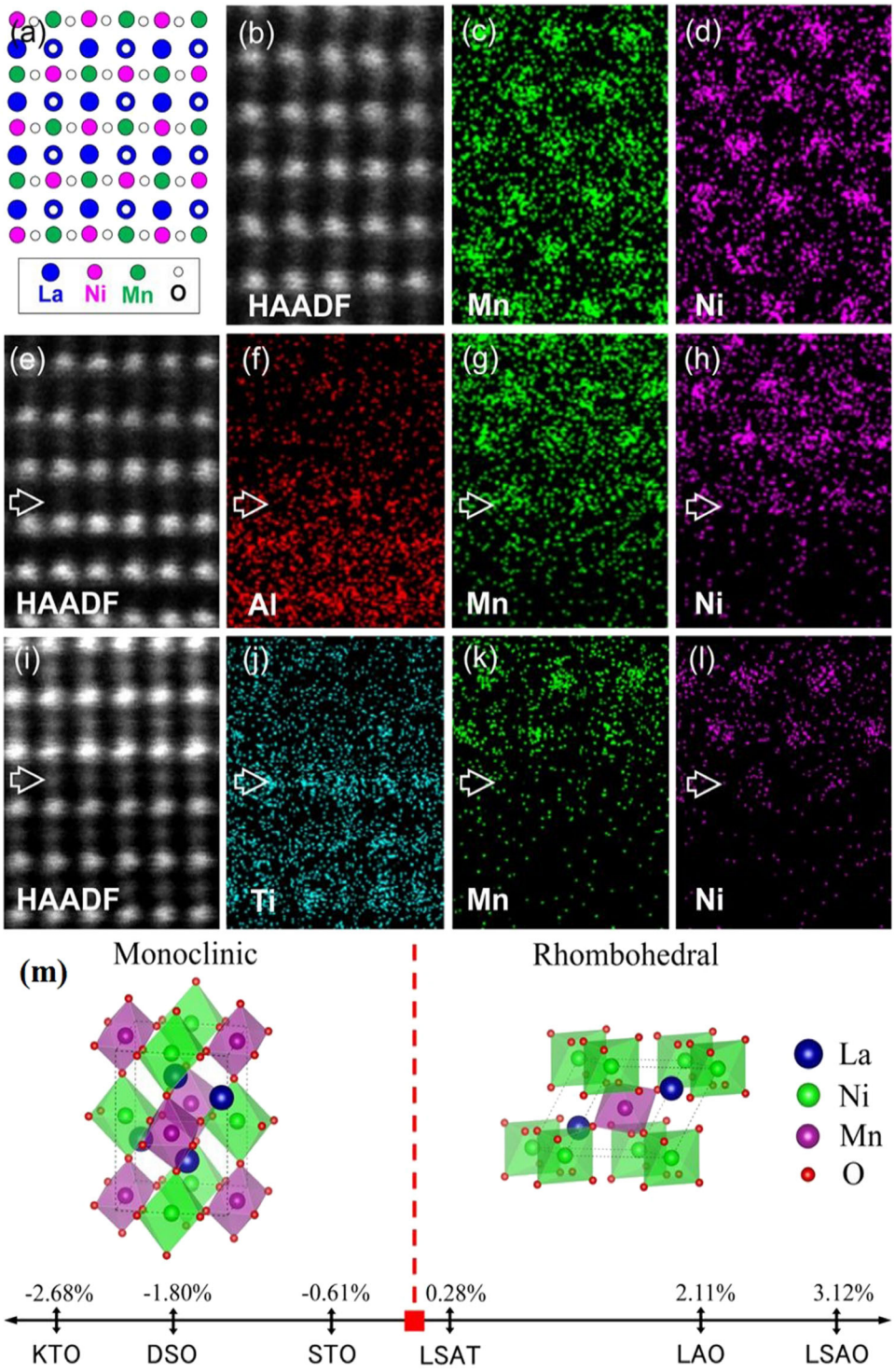

Fig. 7 **a** Model representation of B-site ordered La_2NiMnO_6, (**b**–**d**) Atomic-resolution HAADF image and EDS maps. **e**–**h** HAADF picture of the $La_2NiMnO_6/LaAlO_3$ interface and EDS maps of Al, Mn and Ni. **i**–**l** HAADF picture of the $La_2NiMnO_6/SrTiO_3$ interface and EDS maps of Ti, Mn and Ni. **m** Epitaxial-strain-induced phase transition in La_2NiMnO_6 films [66]

$KTaO_3$ (KTO), $LaAlO_3$ (LAO), and $DyScO_3$ (DSO) using pulsed laser deposition in investigated by advanced electron microscopy and reported as monoclinic and rhombohedral structure of La_2NiMnO_6 films under tensile strain compressive strain, respectively [66]. Thus, they tuned the long-range ordering of B-site cations in La_2NiMnO_6 films in monoclinic and rhombohedral phases (Fig. 7).

4 La_2NiMnO_6 nanoparticle

Two or more simple oxides are present in a perovskite oxide, such high temperature is required to synthesis in single phase which can reduce the surface area. Catalytic properties are highly sensitive to the surface area of perovskite oxides. Thus, material scientist are trying to

Table 2 Annealing temperature T_{ann}, the corresponding particle sizes D obtained from TEM, values of freezing temperature T_P, Curie temperature T_{c1} and T_{c2} from the magnetic curves [67]

T_{ANN}°C	D (NM)	T_P(K)	T_{C1} (K)	T_{C1} (K)
600	16	85	179	141
700	31	75	211	116
800	45	60	268	107
900	57	57	275	103
1000	66	52	284	102

synthesize in alternative way at low temperature. Zhao et al. [67] have prepared La_2NiMnO_6 nanoparticles with sizes lying in the range of 16–66 nm. They have found that with the decrease of particle size the ratio of disordered phase increases, which may be realized from the changes of Curie temperature and the occurrence of glass like properties. The experimental findings have clearly shown that structural and magnetic properties of such material are responsive to the particle sizes (Table 2), which can lead charge disproportion of Mn and Ni of mix valence. In this study it has also been concluded that particle sizes of this materials play a crucial role in determining the ordered and disordered phases [67].

Nanomaterials bear a wide range of potential technological applications [68]. Nanoparticles (NPs) with various structures [68], especially perovskites [69] exhibit a quite dissimilar property as compared with the bulk counterpart. However, bulk La_2NiMnO_6 shows numerous fascinating properties such as colossal magneto-dielectric (~16%) behavior with high ferromagnetic Curie temperature (~280 K) [10]. La_2NiMnO_6 NPs also show numerous interesting properties where nanoscale inhomogeneity or disorder is considered to play the main role in showing ferroelectric and ultimate multiferroic behaviors. In double perovskites, the disorder induced polar property in relaxor ferroelectric or ferroelectric form was determined by Singh et al. [70]. Ferroelectric (relaxor) property is found in La_2NiMnO_6 NPs; whereas bulk counterpart does not show this property [71]. Moreover, La_2NiMnO_6 NPs show a broad relaxor dielectric peak temperature (~220 K), closer to the ferromagnetic transition temperature (FM-Tc ~ 220 K), under a low magnetic field (0.5 T) with a significant improvement of magneto capacitive effect (MC ~ 30%) [71], where the nano-dimension effect plays the vital role by persuading disorder or inhomogeneity. The chemical and valence mixing relating to the surface and anti-site disorders is responsible for the inhomogeneity in ferromagnetic La_2NiMnO_6 NPs. Ferromagnetic transition (~150 K) with low saturation magnetization is obtained by Chandrsekhar et al. [72] from ~27 nm La_2NiMnO_6 NPs due to the existence of anti-site effects. The authors have also reported the frequency-dependent AC susceptibility and exchange bias effects, which conforms the competing interactions, leading to glassy behavior in nanoparticles. A high temperatures paramagnetic insulating phase, low temperatures ferromagnetic insulating phase, and intermediate temperature range Griffiths-like phase in nano crystalline La_2NiMnO_6 was reported by Chakraborty et al. [73]. It has been obtained that the nonlinear AC conductivity is a sensitive probe to recognize various magnetic phases in the system pointing to a significant correlation between electric and magnetic degrees of freedom [74].

5 Applications

Owning to its magnetic and electric properties, La_2NiMnO_6 double perovskites is a promising candidate for novel applications in electronics, energy, environment, and health.

5.1 Applications in solar cell

Hybrid organic inorganic perovskites solar cells have gained a prompt progress after introducing the perovskite solar cell in the place of organic dyes in 2009 [75]. The high-power conversion efficacy of perovskite solar cells (~21%) made it as a potential alternative of conventional silicon solar cells [75–77]. The proper band gap of the perovskites made the hybrid perovskite solar cells appreciable for remarkable light to electricity conversion efficiency. For instance, a system namely methyl ammonium lead iodide ($CH_3NH_3PbI_3$) with band gap of 1.5 eV show high absorption coefficient and carrier mobility and long electron-hole diffusion length up to 175 mm [77], and bipolar carrier transport ability [76, 77]. However, lead based materials possess some detrimental effects, such as the instability of the perovskite materials may result in weak long-term stability of the solar cells and more importantly its toxicity to environment and health [78, 79]. Consequently, stable and less toxic perovskite materials are required in order to overcome these limitations. It is reported that multiferroic inorganic perovskite semiconductors may be an encouraging substitute for solar cell applications [79].

La_2NiMnO_6 double perovskites showing 1.5 eV band gap has been reported by Kitamura et al. [60]. It is easier to synthesize La_2NiMnO_6 double perovskites by simple chemical method than the synthesis of Bi_2CrFeO_6 and $[KNbO_3]_{1-x}[BaNi_{1/2}Nb_{1/2}O_{3-d}]_x$, where in most of the cases complicated method like vapor deposition method is used [80]. Dass et al. [11] and Sun et al. [80]. have characterized the different crystal structures of La_2NiMnO_6 synthesized under different conditions. In such reports it has been obtained that the crystal structures of La_2NiMnO_6 have a profound affect upon their physical properties such as dielectric and magnetic properties [11, 80]. However, there is still quite a lack of research on

electronic properties of different structured La_2NiMnO_6, such as B-site and phase affecting band gap and electronic structures, which is a key factor for solar cell application.

The solar cell application of La_2NiMnO_6 double perovskite considering their electronic structure and band gap was evaluated by Lan et al. [81] theoretically and experimentally. They have synthesized the samples in two different conditions, one sample annealed at 600 °C for 10 h in air (LNM600) and the other at 900 °C keeping the annealing time same in a tube furnace at oxygen atmosphere (LNM900). An energy diagram is shown in Fig. 8 drawn based on band gap and valence states. The conduction bands for both the samples LNM600 and LNM900 are found to be greater than that of ITO and $SrRuO_3$ thin films. The crystal structure has been found to affect the energy level where the monoclinic LNM900 and rhombohedral LNM600 showed energy differences to those of $SrRuO_3$ as 0.8 and 0.7 eV, respectively. Consequently, the photon-excited electron in La_2NiMnO_6 could be injected into $SrRuO_3$ layer, considering $SrRuO_3$ as an appropriate electron conductor [82], which can form a Schottky junction. In case of Bi_2CrFeO_6, the simple ITO/ Bi_2CrFeO_6/$SrRuO_3$ layer-structured Schottky solar cells achieved high-power conversion efficiency, even though there were many defects in Bi_2CrFeO_6. Hence, the band gap and energy level matching aspects clearly demonstrate that La_2NiMnO_6 can function like Bi_2CrFeO_6 in order to fabricate a lead-free perovskite solar cell. The results clearly revealed that monoclinic La_2NiMnO_6 perovskite could be a better alternative than rhombohedral one for light harvesting.

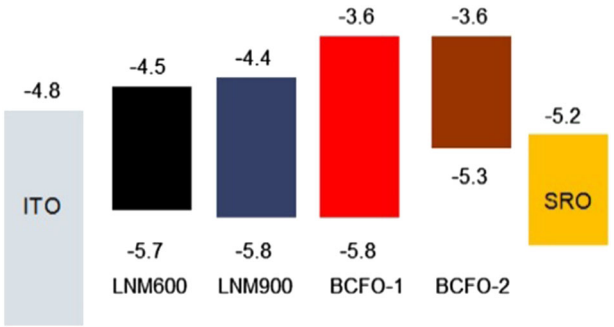

Fig. 8 Energy band diagrams of LNM600, LNM900, and related materials reported [Reprinted with permission from Ref. 81, Copyright 2016, Elsevier, 128]

5.2 Biological applications

Magnetic NPs possess remarkable biological and medical applications [83] like bio-separation [84], antibiotic application [85], quantitative immunoassay [86], and hyperthermia [87]. In recent past, nano-perovskite have drawn a considerable interest to the researchers for their various technological applications [66, 68, 88, 89]. $MnFe_2O_4$, Fe_2O_3, Fe_3O_4, $CoFe_2O_4$, and Fe NPs having magnetic property are extensively used for biomedical applications [90–94]. For the use of La_2NiMnO_6 NPs in the aforementioned fields, the NPs have to be monodispersed in order to interact with the biomolecules like protein. Proteins generally show a tendency to aggregate at the interface between the aqueous solution and solid surfaces [95–99]. Proteins have to be adsorbed on the surface for their applications such as biotechnology, environmental science, and bio-medical engineering. It is noteworthy to mention here that, the adsorbing capability of La_2NiMnO_6 NPs on the bovine serum albumin was reported to be affected by the annealing temperature of La_2NiMnO_6 NPs [100]. The authors reported that bovine serum albumin exhibited a remarkable room temperature adsorbing tendency on magnetic La_2NiMnO_6 NPs. However, the highest adsorbing ability of 219.6 mg/g was obtained for the La_2NiMnO_6 NPs sintered at 850 °C. The adsorbing ability of La_2NiMnO_6 NPs are summarized in Table 3 [100].

5.3 Applications in electric tunable devices

The dielectric tunable materials have drawn a remarkable interest to the researchers because of potential applications of this type of electric devices in this capacitors, phase shifters, microwave communication devices, filters, and oscillators [101, 102]. The high dielectric tunability of conventional ferroelectric substances generally allow them to function under a large DC electric field and to follow temperature dependency around their Curie temperature [103]. Tang et al. [104] have depicted that bulk La_2NiMnO_6 show giant dielectric tunability, which is induced by a comparatively low electric field (40 V/cm) to nearly room

Table 3 Average grain size and magnetic and BSA adsorption properties of La_2NiMnO_6 nanoparticles [15]

Annealing temperature (°C)	Grain size (nm)	MS ($\times 10^{-3}$ emu/g)	H_c (O_e)	Nanoparticle mass (mg)		BSA (mg/g)	Adsorbed
				a	b	a	b
750	33.9	1.97	37.5	5.5	7.8	51.00	36.84
850	36.5	3.1	19.9	6.5	8.2	189.35	219.61
950	37.9	1.97	42.3	5.4	7.2	51.94	30.24
1050	39.6	3.79	39.9	7.1	7.4	27.68	33.04

temperature. Notable dielectric tunability has also been obtained in porous La_2NiMnO_6 ceramic synthesized by gel method using PVA [105]. Its large tunability is also complemented by the high permittivity and loss like ferroelectrics [106]. In addition, modifications of La_2NiMnO_6 have been executed to tuning its behavior. Substitution of La by Sr in La_2NiMnO_6 results a transition to half-metallic phase from ferromagnetic insulating phase [107]. The ferromagnetic $La_2NiMn_{1-x}Ti_xO_6$ is found to be transformed into its antiferromagnetic phase when Mn is substituted by Ti. The dilution effect suppress the dielectric constant and relaxor-like properties [108]. The mixed monoclinic and rhombohedral phases of La_2NiMnO_6 is transformed to only monoclinic phase after Sr–Sb co-doping. Room temperature high-dielectric permittivity and dielectric tunability of Sr–Sb co-doped La_2NiMnO_6 is resulted from the electrode effect [109]. The high dielectric constant and relaxation property has been explained by the local polarization from the charge ordering of Mn^{4+} and Ni^{2+} [104, 110, 111]. However, the intrinsic origin for high dielectric constant of La_2NiMnO_6 was enquired and extrinsic Maxwell–Wagner (M–W) polarization was suggested to report for its irregular dielectric behavior [112]. The presence of internal boundary layers or external depletion layers formation at the interface of the sample/electrode caused by the Schottky barrier effect in the inhomogeneity of microstructure and composition result in M–W polarization of polycrystalline ceramic [113, 114]. However, its applications may be hampered by the external contribution from the depletion layers [114]. For practical application, it is essential to repress its dielectric loss, however, there is a controversy on the source of the high dielectric constant [104, 115]. Non-ferroelectric material such as MgO is added to $Ba_{1-x}Sr_xTiO_3$ to balance the dielectric constant and tenability as a fruitful step [116].

DC voltage dependence of normalized dielectric permittivity at selected frequencies for La_2NiMnO_6 is shown in Fig. 9 [117] and dielectric tunability detected at the low frequency range (<10 kHz). The increasing frequency continuously suppressed the dielectric tunability and disappear nearly at a critical frequency (200 kHz). In an earlier study, Chen et al. [117] have reported the effect of addition of MgO on the microstructure, electrical, and dielectric behavior of La_2NiMnO_6 ceramics. The impedance of $La_2NiMnO_{6-x}MgO$ ceramics is dominated by electrode response nearly room temperature. The high dielectric constant of $La_2NiMnO_{6-x}MgO$ ceramics is resulted from two dielectric relaxations arising out of electrode and grain boundary effects. The dielectric constant is decreased by the addition of MgO. At high temperature and low frequency range, the sizable dielectric tunability is originated from the electrode effect. The electrode response of $La_2NiMnO_{6-x}MgO$ is increased by the addition of MgO to nearly room temperature, enhancing the tunability, and this property is applicable for uses of electric-tunable devices.

5.4 Applications in gas sensing

Biswal et al. [118] have introduced a new direction of use of La_2NiMnO_6 as a sensor of gas using impedance measurements technique. Impedance measurement was done by Lock–in Amplifier. The electrical conduction has been reported to be sensitive to gaseous environments and concentration. The gases are adsorbed at the interfaces of electrodes and grain boundaries constituting space charge. The space charge affects the electrical resistance of the sensor enormously [119]. The investigation on La_2NiMnO_6 at different gaseous (nitrogen, oxygen, argon) atmosphere with different concentrations of the gases at different stable temperatures as shown in Fig. 10 have suggested strong dependency of the resistance value with the concentration of

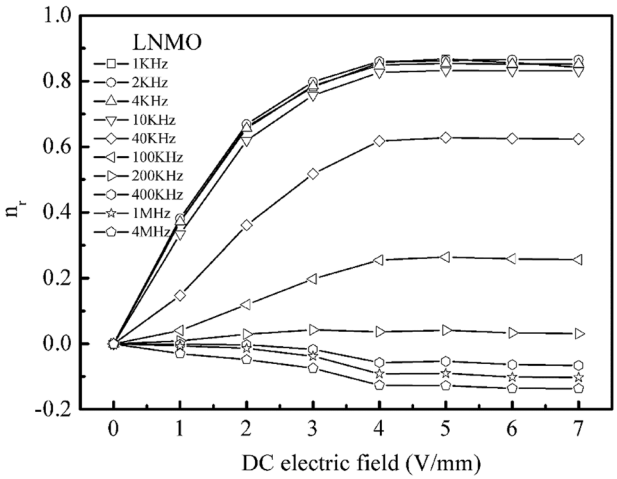

Fig. 9 The DCB voltage dependence of relative tunability (n_r) at selected frequency for La_2NiMnO_6 ceramics [Reprinted with permission from Ref. 117, Copyright 2014, Elsevier]

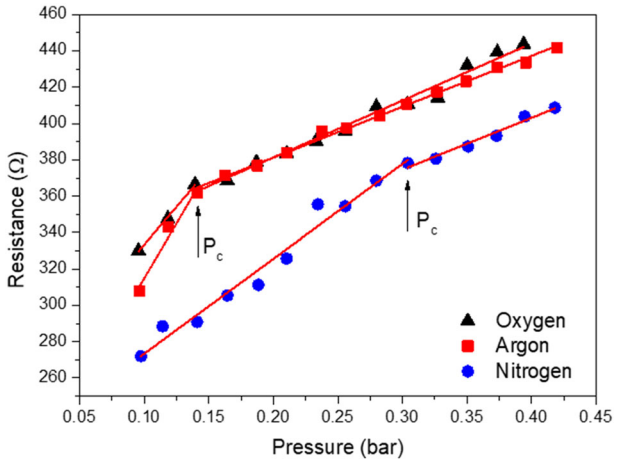

Fig. 10 Resistance versus gas concentration for the three gases. The arrow marks the critical pressure (Pc) at which the slope changes distinctly. The red lines show the linear fit [Reuse the data from the Ref. 118]

gases. In addition, at critical gas pressure (P_c), resistance increases with sharp change in slope as concentration of gas is increased. It has been found that below P_c the sensitivity (slope change) is more and among above mentioned three gases it is maximum for argon. At elevated temperatures resistance values show two dissimilar activated regimes of distinct activation energies. At 1 Tesla magnetic field nitrogen shows nearly zero, oxygen shows a positive and argon shows a negative value of magneto impedance. The maximum magnetoimpedance value of ~ 5% (in magnitude) is found under 1 T magnetic field. Thus, in near future, the sensing device can be fabricated by making thin films of La_2NiMnO_6 and the gas sensing can be elaborated to gas concentrations at ppm level or for various toxic gases.

6 Conclusion and future prospects

La_2NiMnO_6 is a multifunctional oxide with a double perovskite structure showing simultaneous electric and magnetic ordering which have been studied for a last few years as next-generation electronic appliances [120–127]. The charge ordering involves at B-site due to the presence of Ni^{2+}–O–Mn^{4+} electronic interaction which is responsible for the ferromagnetism, magnetoresistance, magneto capacitance, and semi-conductivity. Characteristic features of La_2NiMnO_6 such as crystal structure, electrical, magnetic, and magneto-transport properties are discussed and correlated to establish the mechanism of its action. The emphasis has been given how temperature and magnetic field alters magnetoelectric and electronic behavior of such material. Earlier studies have revealed that the morphology of this material in the form of bulk phase, thin layer, and nanoparticles affect its physical characteristics considerably [124]. The shell surface corelated with grain size, which leads to relaxation of superexchange at the surface with reducing of particle size. The transition metal-oxygen bond angle in La_2NiMnO_6 decreases with the reduction of particle size, which is mainly corelated with magnetic and electrical properties. The present review clearly depicts an idea why the application of La_2NiMnO_6 substituting conventional substances in solar cells, electric tunable devices, biomolecular and gas sensing technologies is advantageous. The focus of this article is to gather all such physical behavior of La_2NiMnO_6 to find its possible beneficial applications in new arena of material research, which may also be directive of future research in double perovskite materials.

Compliance with ethical standards

Conflict of interest The authors declare that they have no conflict of interest.

References

1. Kimura T, Goto T, Shintani H, Ishizaka K, Arima T, Tokura Y (2003) Nature 55:426
2. Hill NA (2000) J Phys Chem B 104:6694
3. Kimura T, Sekio Y, Nakamura H, Seigrist T, Ramirez AP (2008) Nat Mater 7:291
4. Subramanian MA, He T, Chen J, Rogado N S, Calvarese T G, Sleight A W (2006) Adv Mater 18:1737
5. Yang C-H, Lee S-H, Koo TY, Jeong YH (2007) Phys Rev B 75:140104. (R)
6. Ramesh R, Spaldin NA (2007) Nat Mater 6:21
7. Anderson MT, Greenwood KB, Taylor GA, Poeppelmeier KR (1993) Prog Solid State Chem 22:197
8. Goodenough JB (1955) Phys Rev 100:564
9. Kanamori J (1959) J Phys Chem Solids 10:87
10. Rogado NS, Li J, Sleight AW, Subramanian MA (2005) Adv Mater 17:2225
11. Dass RI, Yan J-Q, Goodenough JB (2003) Phys Rev B 68:064415
12. Yue-Lei Z, Yi-Sheng C, Li-Qing P, Young S (2013) Chin Phys B 22:087601
13. Iliev MN, Gospodinov MM, Singh MP, Meen J, Truong KD, Fournier P, Jandi S (2009) J Appl Phys 106:023515
14. Davies PK, Wu H, Borisevich AY, Molodetsky IE, Farber L (2008) Ann Rev Mater Res 38:369
15. Goodenough JB, Dass RI (2000) Int J Inorg Mater 2:3
16. Wold A, Arnott RJ, Goodenough JB (1958) J Appl Phys 29:387
17. Choudhury D, Mandal P, Mathieu R, Hazarika A, Rajan S, Sundaresan A, Waghmare UV, Knut R, Karis O, Nordblad P, Sarma DD (2012) Phys Rev Lett 108:127201
18. Bull CL, Gleeson D, Knight KS (2003) J Phys Condens Matter 15:4927
19. Sayed FN, Achary SN, Jayakumar OD (2011) J Mater Res 26:567
20. Ullah M, Khan SA, Murtaza G, Khenata R, Ullah N, Omran SB (2015) J Magn Magn Mater 377:197
21. Wu Z, Cohen RE (2006) Phys Rev B 73:235116
22. Blascoa J, S nche MC, re -Cacho, Garc a, Sub as G, Campo J (2002) J Phys Chem Solids 63:781
23. Goodenough JB, Wold A, Arnott RJ, Menyuk N (1961) Phys Rev 124:373
24. Blasse G (1965) J Phys Chem Solids 26:1969
25. Blasco J, Garacia J, Sanchez MC, Campo J, Subias G, Perz-Cacho J (2002) Eur Phys J B 30:469
26. Ritter C, Ibarra MR, De Teresa JM, Algarabel PA, Marquina C, Blasco J, García J, Oseroff S, Cheong S-W (1997) Phys Rev B 56:8902
27. Sánchez RD, Causa MT, Sereni J, Vallet-Regí M, Sayagués MJ, González-Calbet JM (1993) J Alloys Compounds 191:287
28. Asai K, Sekizawa H, Iida S (1979) J Phys Soc Japan 47:1054
29. Matar SF, Subramanian MA, Villesuzanne A, Eyert V, Whangbo M-H (2007) J Magn Magn Mater 308:116
30. Zhu M, Lin Y, Lo EWC, Wang Q, Zhao Z, Xie W (2012) Appl Phys Lett 100:062406
31. Truong KD, Singh MP, Jandl S, Fournier P (2009) Phys Rev B 80:134424
32. Kang JS, Wi SC, Lee SS, Kim G, Yang HM, Lee BW, Han SW, Kim KH, Sekiyama A, Kasai S, Suga S, Shim JH, Min BI (2004) J Phys Condens Matter 16:S5685

33. Booth RJ, Fillman R, Whitaker H, Nag Abanti, Tiwari RM, Ramanujachary KV, Gopalakrishnan J, Lofland SE (2009) Mater Res Bull 44:1559
34. Singh MP, Grygiel C, Sheets WC, Boullay Ph, Hervieu M, Prellier W, Mercey B, Simon Ch, Raveau B (2007) Appl Phys Lett 91:012503
35. Joly VLJ, Joy PA, Date SK, Gopinath CS (2002) Phys Rev B 65:184416
36. Chandrasekhar KD, Das AK, Venimadhav A (2012) J Phys Condens Matter 24:376003
37. Iliev MN, Guo H, Gupta A (2007) Appl Phys Lett 90:151914
38. Zhou S, Shi L, Yang H, Zhao J (2007) Appl Phys Lett 91:172505
39. Nair HS, Swain DA, Hariharan N, Adiga S, Narayana C, Elzabeth S (2011) J Appl Phys 110:123919
40. von Helmolt R, Wecker J, Holzapfel B, Schultz L, Samwer K (1993) Phys Rev Lett 71:331
41. Hwang HY, Cheong S-W, Ong NP, Batlogg B (1996) Phys Rev Lett 77:2041
42. Kobayashi K-I, Kimura T, Sawada H, Terakura K, Tokura Y (1998) Nature 395:677
43. Sarma DD, Ray Sugata, Tanaka K, Kobayashi M, Fujimori A, Sanyal P, Krishnamurthy HR, Dasgupta C (2007) Phys Rev Lett 98:157205
44. Du CH, Adur R, Wang HL, Hauser AdamJ, Yang FY, Hammel PChris (2013) Phys Rev Lett 110:147204
45. Hashisaka M, Kan D, Masuno A, Takano M, Shimakawa Y, Terashima T, Mibu K (2006) Appl Phys Lett 89:032504
46. Wang XJ, Sui Y, Li Y, Li L, Zhang XQ, Wang Y, Liu ZG, Su WH, Tang JK (2009) Appl Phys Lett 95:252502
47. Zhou SM, Guo YQ, Zhao JY, Zhao SY, Shi L (2010) Appl Phys Lett 96:262507
48. Garc a-Hernande M, Mart ne L, Mart ne -Lope M, Casais MT, Alonso JA (2001) Phys Rev Lett 86:2443
49. Singh VN, Majumdar P (2011) EPL 94:47004
50. Guo Y, Shi L, Zhou S, Zhao J, Liu W (2013) Appl Phys Lett 102:222401
51. Mostovoy M, Scaramucci A, Spaldin NA, Delaney KT (2010) Phys Rev Lett 105:087202
52. Kitagawa Y et al. (2010) Nat Mater 9:797
53. Fiebig M (2005) J Phys D 38:R123
54. Shvartsman VV et al. (2008) Phys Rev Lett 101:165704
55. Choudhury D et al. (2011) Phys Rev B 84:125124
56. Singh MP, Grygiel C, Sheets WC, Boullay Ph, Hervieu M, Prellier W, Mercey B, Simon C, Raveau B (2007) Appl Phys Lett 91:012503
57. Boullay P, Grygiel C, Rautama EL, Singh MP, Kundu AK (2007) Mater Sci Eng B 144:49
58. Guo H, Burgess J, Street S, Gupta A, Calvarese TG, Subramanian MA (2006) Appl Phys Lett 89:022509
59. Guo HZ, Burgess J, Ada E, Street S, Gupta A, Iliev MN, Kellock AJ, Magen C, Varela M, Pennycook SJ (2008) Phys Rev B 77:174423
60. Kitamura M, Ohkubo I, Kubota M, Matsumoto Y, Koinuma H, Oshima M (2009) Appl Phys Lett 94:132506
61. Singh MP, Simon C, Raveau B, Prellier W (2006) Appl Phys Lett 89:022509
62. Singh MP, Truong KD, Fournier P (2007) Appl Phys Lett 91:042504
63. Padhan P, Guo HZ, LeClair P, Gupta A (2008) Appl Phys Lett 92:022909
64. Singh MP, Truong KD, Jandl S, Fournier P (2009) Phys Rev B 79:224421
65. Mitchell RG (2004) Perovskites. Modern and Ancient Almaz Press, Canada Chap. 1
66. Wu S-Q, Cheng S, Lu L, Liu M, Jin X-W, Cheng S-D, Mi S-B (2018) Sci Rep 8:2516
67. Zhao S, Shi L, Zhou S, Zhao J, Yang H, Y. (2009) J Appl Phys 106:123901
68. Hossain A, Bandyopadhyay P, Guin PS, Roy S (2017) Appl Mat Today 9:300
69. Hossain A, Ghosh D, Dutta U, Walke PS, Mordvinova NE, Lebedev OI, Sinha B, Pal K, Gayen A, Kundu AK, Seikh M (2017) J Magnetis Mag Mat 444:68
70. Singh DJ, Park CH (2008) Phys Rev Lett 100:087601
71. Masud MG, Ghosh A, Sannigrahi J, Chaudhuri BK (2012) J Phys Condens Matter 24:295902
72. Chandrsekhara KD, Das AK, Venimadhav A (2012) AIP Conf Proc 1447:1237
73. Chakraborty D, Nandi UN, Jana D, Masud MdG, Giri S (2015) J Appl Phys 118:035103
74. Zhao S, Shi Lei, Zhou S, Zhao J, Yang H, Guo Y (2009) J Appl Phys 106:123901
75. Kojima A, Teshima K, Shirai Y, Miyasaka T (2009) J Amer Chem Soc 131:6050
76. Yang WS, Noh JH, Jeon NJ, Kim YC, Ryu S, Seo J, Seok SI (2015) Science 348:1234
77. Dong Q, Fang Y, Shao Y, Mulligan P, Qiu J, Cao L, Huang J (2015) Science 347:967
78. Kazim S, Na eeruddin MK, Gr€at el M, Ahmad S (2014) Angew Chem Int Ed 53:2812
79. Gao P, Gr€at el M, Nazeeruddin MK (2014) Energy Environ Sci 7:2448
80. Zhang Z, Jian H, Tang X, Yang J, Zhu X, Sun Y (2012) Dalton Trans 41:11836
81. Lan C, Zhao S, Xu T, Ma J, Hayase S, Ma T (2016) J Alloys Compd 655:208
82. Bern F, Ziese M, Setzer A, Pippel E, Hesse D, Vrejoiu I, Physics J (2013) Cond Matter 25:496003
83. Eerenstein W, Mathur ND, Scott JF (2006) Nature 442:759
84. Ito A, Shinkai M, Honda H, Kobayashi T (2005) J Bios Bioeng 100:1
85. Atique Ullah AKM, Kabir MF, Akter M, Tamanna AN, Hossain A, Tareq ARM, Khan MNI, Fazle Kibria AKM, Kurasaki Masaaki, Rahman MM (2018) RSC Adv 8:37176–37183
86. Tang DP, Yuan R, Chai YQ (2006) J Phys Chem B 110:11640
87. Banerjee R, Katsenovich Y, Lagos L (2010) Curr Med Chem 2010:3120
88. Kim WS, Anoop G, Lee HJ, Su Lee S, Kwak JH, Lee H, Jo JY (2016) J Cat 344:578
89. Haider MA, Capizzi AJ, Murayama M (2011) Steven McIntosh Solid State Ionics 196:65
90. Tang IM, Krishnamra N, Charoenphandhu N, Hoonsawat R, Pon-O W (2011) Nanoscale Res Lett 6:19
91. Mornet S, Vasseur S, Grasset F, Veverka P, Goglio G, Demourgues A, Portier J, Pollert E, Duguet E (2006) Prog Solid State Chem 34:237
92. Fan HM, Yi JB, Yang Y (2009) ACS Nano 3:2798
93. Kim HJ, Ahn JE, Haam S (2006) J Mater Chem 16:1617
94. Ruan J, Ji JJ, Song H, Qian QR, Wang K, Wang C, Cui DX (2012) Nanoscale Res Lett 7:309
95. Kopac T, Bozgeyik K, Yener J (2008) Colloids Surfactants A 322:19
96. Rezwan K, Meier LP, Gauckler LJ (2005) Biomaterials 26:4351
97. Rezwan K, Studart AR, Voros J (2005) J Phys Chem B 109:14469
98. Seitz R, Brings R, Geiger R (2005) Appl Surf Sci 252:154
99. Hollmann O, Czeslik C (2006) Langmuir 22:3300
100. Wu Z-Y, Ma C-B, Tang X-G, Li R, Liu Q-X, Chen B-T (2013) Nanoscale Res Lett 8:207
101. Kleemann W, Dec J, Wang R, Itoh M (2003) Phys RevB 67:092107
102. Liang X, Wu W, Meng Z (2003) Mater Sci Eng B 99:366

103. Maiti T, Guo R, Bhalla AS (2007) Appl Phys Lett 90:182901
104. Tang MH, Hou JW, Zhang J, Dong GJ, Shu W (2010) Solid State Comm. 50:1453
105. Li C, Liu B, He Y, Lv C, He H, Xu Y (2014) J Alloys Compd 590:541
106. Tagantsev AK, Sherman VO, Astafiev KF, Venkatesh J, Setter N (2003) J Electroceram 11:5
107. Kim B, Choi HC, Kim BH, Min BI (2010) Phys Rev B 81:224402
108. Yang WZ, Liu XQ, Lin YQ, Chen XM (2011) J Appl Phys 111:084106
109. Cao Z, Li Z, Gao Y, Liu J, Ruan X, Fang M (2014) Phys Status Solidi 211:1207
110. Gavin L (2012) Physics 5:35
111. Lin YQ, Chen XM, Liu XQ (2009) Solid State Commun 149:784
112. Chandrasekhar KD, DAS AK, Mitra C, Venimadhav A (2012) J Phys 24:495901
113. Hippel ARVon (1966) Dielectrics and Waves. MIT Press, Cambridge
114. Wang CC, He M, Yang F, Wen J, Liu GZ, Lu HB (2007) Appl Phys Lett 90:192904
115. Yu J, Ishikawa T, Arai Y, Yoda S, Itoh M, Saita Y (2005) Appl Phys Lett 87:252904
116. Agrawal S, Manuspiya H, Guo R, Agrawal D, Bhalla AS (2004) Ceram Trans 150:299
117. Chen H, Cao Z, Wang L, He W, Sun J, Zhang Y, Ruan X (2014) J Alloys Compd 616:213
118. Biswal AK, Ray J, Kuila S, Vishwakarma PN (2015) Vol. 1665, AIP Conference Proceedings, p 140050, AIP Publishing LLC, NY USA
119. Labidi A, Jacolin C, Bendahan M, Abdelghani A, Guerin J, Aguir K, Maaref M (2005) Sensor Sensor Actuat B-Chem 106:713
120. Orlandi F, Righi L, Ritter C, Pernechele C, Solzi M, Cabassi R, Bolzoni F, Calestani G (2014) J Mat Chem C 2:9215
121. Hossaina A, Bandyopadhyay P, Roy S (2018) J Alloys Comd 740:414
122. Atique Ullah AKM, Kibria AKMF, Akter M, Khan MNI, Maksud MA, Jahan RA, Firoz SH (2017) J Saudi Chem Soc. 21:822
123. Gilev AR, Hossain A, Kiselev EA, Cherepanov VA (2018) Solid State Ionics 323:64–71
124. Karimunnesa S, Ullah AKMA, Hasan MR, Shanta FS, Islam R, Khan MNI (2018) Effect of holmium substitution on the structural, magnetic and transport properties of $CoFe_{2-x}Ho_xO_4$ ferrites. J Magn Magn Mater 457:57
125. Dutta Uma, Hossain Aslam, Walke PravinS, Ghosh Debamalya, Mordvinova NataliaE, Lebedev OlegI, Haque Ariful, Pal Kamalesh, Gayen Arup, Kundu AsishK, Seikh MdMotin (2019) J Alloys Compd 777:1396
126. Hossain Aslam, Roy Sanjay, Sakthipandi K (2019) Ceram Int 45:4152
127. Atique Ullah AKM, Hossain A, Akter M, Kabir MF, Khan MNI, Kibria AKMFazle, Firoz ShakhawatH (2019) Mater Lett 238:151
128. Nechache R, Harnagea C, Li S, Cardenas L, Huang W, Chakrabartty J, Rosei F (2015) Nat Photonics 9:61
129. Masud MG, Ghosh A, Sannigrahi J, Chaudhuri BK (2012) J Phys Condens Matter 24:295902
130. Kumar P, Ghara S, Rajeswara B, Muthu DVS, Sundaresan A, Sood AK (2014) Solid State Commun 184:47